VOL. 16, NO. 4, FEBRUARY 2021 ISSN 1819-6608
ARPN Journal of Engineering and Applied Sciences

www.arpnjournals.com

PROPOSAL FOR A NEURO-FUZZY SYSTEM FOR UVEAL MELANOMA DETECTION

Daniel F. Santos-Bustos and Helbert E. Espitia-Cuchango
Facultad de Ingeniería, Universidad Distrital Francisco Joséde Caldas, Bogotá, Colombia
E-Mail: heespitiac@udistrital.edu.co

ABSTRACT

This paper presents a proposal for a Neuro-Fuzzy system to detect cancer-type Uveal Melanoma (UM). The proposed method integrates image processing algorithms with neuro-fuzzy system to detect the Uveal Melanoma. The results present the training process for two configurations of the neuro-fuzzy system. Rules that are redundant in the system could be identified and simplified. The model created using ANFIS provides a suitable system for the detection of Uveal Melanoma obtaining results close to 90.2% of accuracy.

Keywords: cancer, image processing, neuro-fuzzy, uveal melanoma.

1. INTRODUCTION

Cancer in its different locations and variants is a public health problem worldwide. According to the National Cancer Institute (NIH), this is one of the leading causes of death around the world. In 2012, there were 14.1 million new cases and 8.2 million deaths related to cancer. It is anticipated that by 2030 the number of new cases will increase to about 23.6 million [1]. Life expectancy is increasing in countries due to better control of infectious, parasitic and perinatal diseases as well as the proportion of people of more advanced age increases, in whom the incidence of cancer is higher.

However, as Mayer Zaharia mentions in [2], around 80% of cancer patients who attend to a specialized consultation do this in advanced stages of the disease, to whom treatment is difficult with high cost, and with low performance.

One of the ways to reduce the death rate by cancer, according to Miller in [3] is through an adequate orientation of public policies, particularly in prevention policies and early diagnosis. Early diagnosis followed by treatment allows curing more than 50% of cancer cases.
The Uveal Melanoma (UM) is a type of intraocular cancer that arises in the melanocytes of the iris, the ciliary body or the choroid. Early diagnosis and local treatment are crucial since survival rates correlate with the size of the primary tumor. However, approximately 50% of patients will develop metastases with survival of 6-12 months from diagnosis [4].

According to [5] 3 out of 4 people with ocular melanoma survive for at least 5 years. Survival rates tend to be better for cancer in earlier stages than for those in later stages. When cancer is confined to the eye, the related survival rate after 5 years is around 80%. For people with eye melanomas that have spread to distant parts of the body, the 5-year related survival rate is around 15%. Related works are focus on examining patterns, colors, and other characteristics of the iris to determine the health of the patients [6], [7]. In [8] is shown a proposal to detect diseases in the iris using the Gabor filter, allowing the classification of Corneal Oedema, Iridotomies and Conjunctivitis. In [9] using the transformation of ‘‘Watershed’’ and the iris characteristics, it was developed a proposal for detection of kidney problems. A description of different examples of ciliary body melanoma can be seen in [10].

On the other hand, image processing allows extracting features from a picture to be used in the classification process, additionally; neuro-fuzzy systems have the capability to transform a dataset of information into a set of rules.

In this paper, image processing and a neuro-fuzzy structure are used for proposing a system for identifying UM considering that early detection significantly increases the chances of survival. Figure-1 shows the scheme of the proposed system.

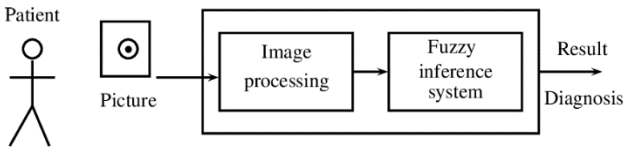

Figure-1. Scheme of the proposed system.

2. MATERIALS AND METHODS

2.1 Takagi-Sugeno Fuzzy Systems and ANFIS

According to [11] fuzzy logic represents information of complex systems in terms of fuzzy sets, given an input to obtain the output the sets are combined in rules. By using learning algorithms, the fuzzy systems are optimized obtaining information from a data set. Based on [11] and [12] as starting point for the optimization process, preliminary knowledge employed can be used to design the fuzzy system. A classic if-then fuzzy rule is described as:

If the proposition (in the antecedent) x *then,* proposition (in the consequent) z.

A feature of x corresponds to a linguistic label and is represented by a fuzzy set $\mu(x)$ function of the input x [12].

Considering [13] the Mamdani fuzzy systems allow the representation of knowledge using fuzzy sets for

inputs and outputs. On the other hand, the Takagi-Sugeno model uses a function that depends on inputs. However, it is possible a relation between Mamdani and Takagi-Sugeno systems using a constant function that is equivalent in Mamdani model using a singleton set [14]. This characteristic can be used to extend a Takagi-Sugeno into a Mamdani model.

According to [14] using input-output dataset the Takagi-Sugeno fuzzy systems provides a method for generating fuzzy rules. Considering A and B like a fuzzy sets in the antecedent with associated membership functions μ_A and μ_B then an example of Takagi-Sugeno rule is:

Ifx is A and y is B**then**$z = f(x, y)$

In some applications, polynomial functions are used for $f(x, y)$ having:

- Zero-order model: $f = a$.
- First-order model: $f = ax + by + c$.
- Second-order model: $f = ax^2 + by^2 + cxy + dx + ey + g$.

To provide the adaptability to fuzzy systems is developed the Adaptive Neuro-Fuzzy Inference System (ANFIS). This focus allows the representation of a fuzzy system like a neural network to perform the training using input-output data. To achieve this feature is used the Takagi-Sugeno fuzzy model [14].

In order to show an example of ANFIS is considered a first-order Takagi-Sugeno model with two inputs x and y and one output z. The example rules are:

- **Inference rule 1:** *If*x is A_1 and y is B_1, *then*$f_1 = a_1x + b_1y + c_1$
- **Inference rule 2:** *If*x is A_2 and y is B_2, *then*$f_2 = a_2x + b_2y + c_2$

Figure-2 shows the respective example of TSK fuzzy system and Figure-3 the neural structure associated with the fuzzy system.

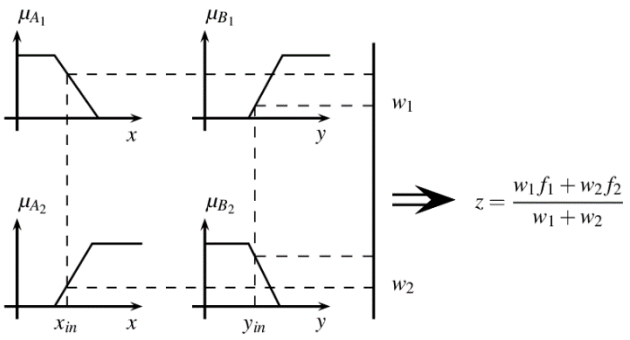

Figure-2. Example of TSK fuzzy system using two membership functions in each input.

Considering the described in [14] the function of each layer in the neural representation is:

- **Layer 1:** An adaptive layer where the fuzzification process is performed. The output is the value of the evaluated membership function.
- **Layer 2:** Each node represents a rule. This layer corresponds to the fuzzy relation process between membership functions.
- **Layer 3:** Here, the normalization process is performed. The result corresponds to the normalized weights.
- **Layer 4:** An adaptive layer where the multiplication between normalized weights and the input functions are computed.
- **Layer 5:** This layer is associated to defuzzification process. Here, the overall output is computed as the sum of all incoming signals.

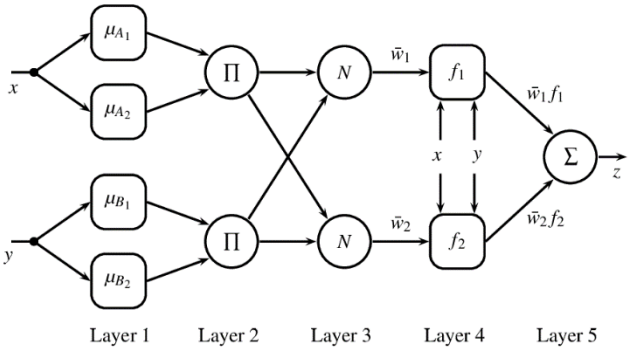

Figure-3. Example of ANFIS system, showing the neural net associated to the fuzzy system.

In this work, a Takagi-Sugeno model is used as it employs data for adjustment of fuzzy model. To obtain more interpretability, this model can be extended into a Mamdani fuzzy system; according to [14] a zero-order TSK fuzzy model is related to Mamdani Fuzzy models that employ singleton sets in the consequent. An alternative to this conversion consists of the use of constant functions for TSK and consequently extent the associated singleton set to a Gaussian function in a Mamdani model, this process permits having fuzzy sets in the inputs and output, increasing the interpretability. Another relevant aspect to obtain a suitable fuzzy model is the mechanism to simplify rules, as in ANFIS model the rules consists of the combination of all fuzzy sets used in the inputs. The simplification process is achieved using the weight value associated with each rule.

ANFIS has been used in a variety of applications such as short-term wind forecasting, [15], stock market forecasting [16], project evaluation [17], time series of regional electricity loads [18] and classification tasks like the one in [19]. The proposal showed in this paper can be considered as an approximation to have a system with information that allows the Uveal Melanoma detection using zero-order TSK fuzzy models. Additional works can be oriented to convert TSK to Mamdani model and the simplification of inference rules.

2.2 Image Processing Used

The employed algorithm is divided into the sub-stages showed in Figure-4. To train and test the system proposed the images of CASIA [20] and the images of the page of the eye cancer center in New York [21] were used.

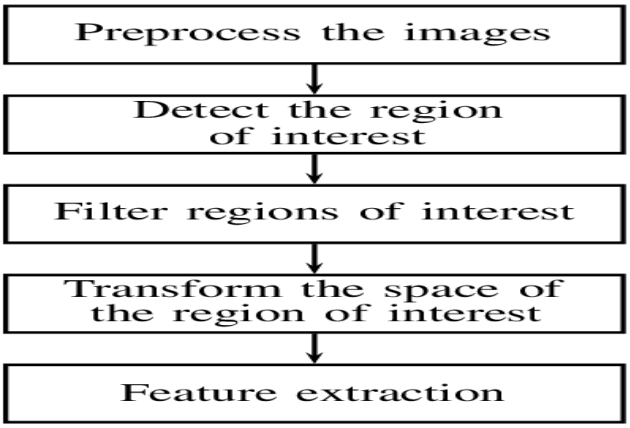

Figure-4. Stages of the proposed system whose purpose is to get the features of images with and without Uveal Melanoma.

2.2.1 Images preprocessing

The algorithm of Figure-5 was used in this stage, where it is sought to remove noise from the image in order to facilitate the detection of the (ROI) in the next stage.

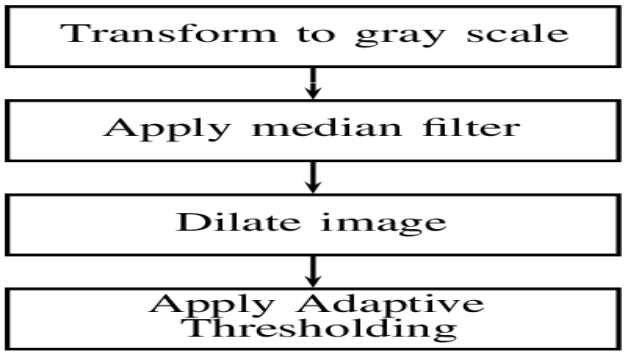

Figure-5. Stages for Image preprocessing. Used to facilitate the detection of the Region of Interest (ROI) in the system proposed.

Conventional thresholding methods use a threshold for all pixels, while Adaptive Thresholding (AT) changes the threshold value dynamically on the image. The AT has shown better results concerning the traditional thresholding since the illumination and the shadows change depending on the position of the image [22]. For example, Figure-6 shows a suspicious Iris Nevus, where the ectropionuveae, correctopia, and the variable brown are observed.

Figure-7 presents the results of preprocessing, part (a) the image in gray scale, part (b) gray image after applying a median filter. Part (c) the image after applying the adaptative thresholding. Finally, part (d), the dilate image.

As comparison example, Figure-8 shows the results of preprocessing healthy eye form CASIA Database [20]. Part (a) shows the image in gray scale. Part (b) the gray image after applying a median filter. Part (c) image after applying the adaptative thresholding. Finally part (d), the dilate image.

Figure-6. Suspicious Iris Nevus. Note the ectropionuveae, correctopia and the variable brown and ‘‘tapioca’’ coloration. Source [21].

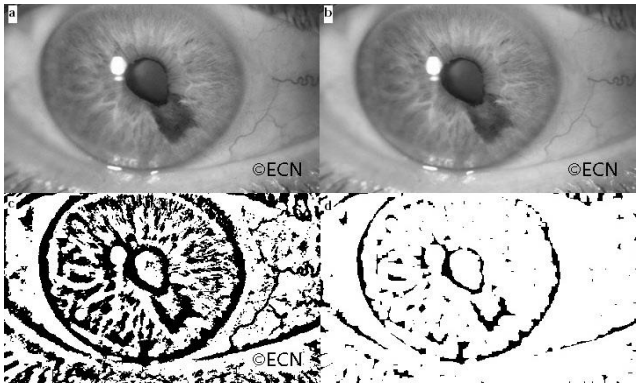

Figure-7. Results stages of preprocessing of Figure-6. (a) Image in gray scale. (b) Gray image after applying a median filter. (c) Image after applying the adaptative thresholding. (d) Dilate image.

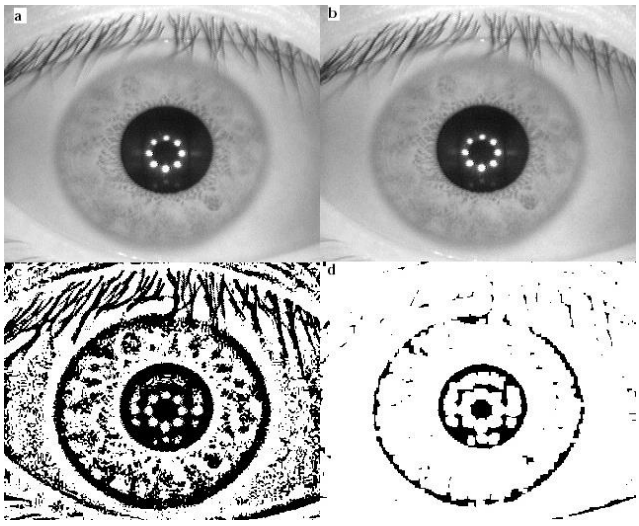

Figure-8. Results stages of preprocessing healthy eye CASIA Database. (a) Image in gray scale. (b) Gray image after applying a median filter. (c) Image after apply the adaptative thresholding. (d) Dilate image. Source [20].

2.2.2 Detection of the region of interest

In this stage, the Hough transform is used to detect circles. This is an algorithm used to search circles in images; this approach is used since it provides robustness in the presence of noise, occlusion and variation of illumination [23]. This algorithm has three fundamental phases which are shown in Figure-9.

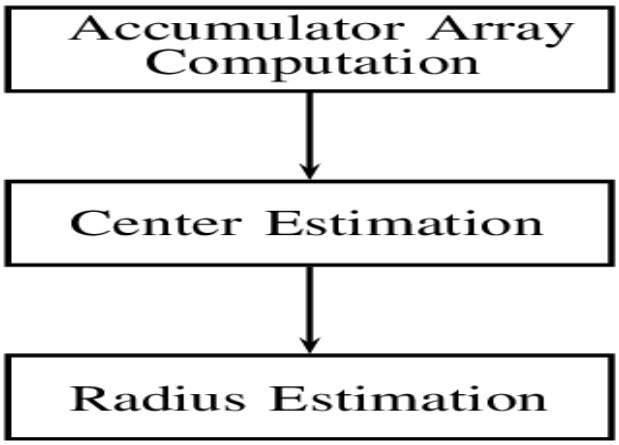

Figure-9. CHT algorithm fundamental phases to detect circles in images.

The CHT is used to transform a set of characteristics of points in the space of the image to a set of votes accumulated in the space of the parameters; these votes are integer values that are stored in an array. The position of the arrangement that contains the higher number of votes indicates the presence of a circle. In this process, different arguments of the transform are changed and applied multiple times to the images obtained in the preprocessing stage.

2.2.3 Filtering regions of interest

Since the previous stage the arguments of the transformation were varied, repeated or very close circles were generated, therefore, filtering rules and data structures are used: Binary trees and Union Find by rank and path compression help to reduce these problems. This algorithm is implemented in the detected regions of interest to reduce the processing time in later stages and increment the accuracy. The regions of interest detected and the results after filtering those regions are shown in Figures 10 and 11.

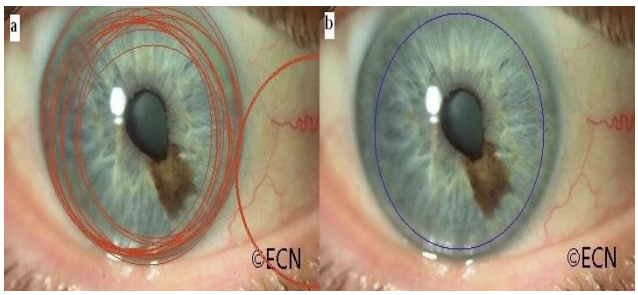

Figure-10. Results of the detected regions of interest detected from Figure-6. (a) All regions of interest detected. (b) Filtered regions of interest using algorithms and data structures.

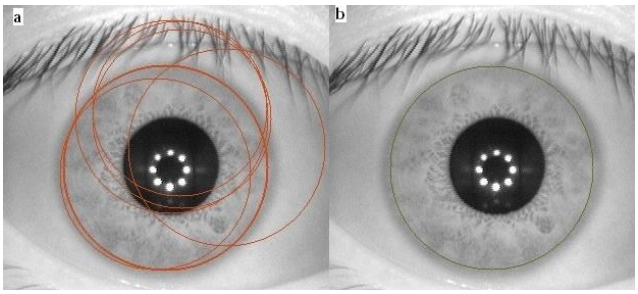

Figure-11. Results of the detected regions of interest detected. (a) All regions of interest detected. (b) Filtered regions of interest using algorithms and data structures.

2.2.4 Transformation of space of the region of interest

Since non-iris pixels is noise for the present case study, it is important to isolate the region of interest and find the characteristics of these. After that process, the iris is transformed into a rectangle allowing removing the noise produced by the sclera, eyelid, and eyelashes. The results of this stage are shown in Figures 12 and 13.

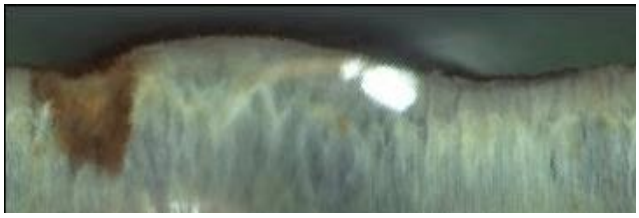

Figure-12. Transformed detected region of interest to cartesian coordinates.

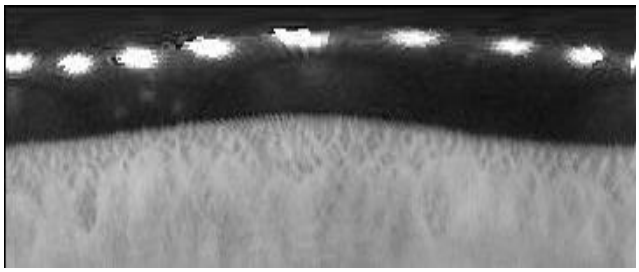

Figure-13. Transformed detected region of interest to cartesian coordinates.

2.2.5 Feature extraction

For the extraction of features the Hu moments were selected due to their properties for identification. The moments have been widely applied for pattern recognition in images due to their properties [24]. The seven invariants are very useful properties that do not change in scale, translation and rotation, for that reason they have been widely used to perform pattern recognition, image registration and image reconstruction [24].

The invariants of Hu moments can be calculated using the central moments, which are defined by equation (1). The moments μ_{pq} are calculated using the image $f(x, y)$, where $p, q = 0,1,2,3$ ...

$$\mu_{pq} = \sum_{x=1}^{M} \sum_{y=1}^{N} (x - x')^{p} (y - y')^{q} f(x, y) \quad (1)$$

The extraction was made on a total of 1622 images. Using these images, the features were extracted and stored in a comma-separated value file (csv), which will be later used to perform the neuro-fuzzy classifier.

2.3 Neuro-fuzzy system design

Two configurations using 2 and 3 membership functions in each input are used for the implementation of the neuro-fuzzy system. This model allows the representation of knowledge using logic rules. The inputs to the system are the seven moments of Hu h_0, h_1, h_2, h_3, h_4, h_5, h_6, and the output the respectivediagnostic, namely healthy or unhealthy.

In this work, Gaussian functions were used since they are derivable and therefore allow the implementation of learning algorithms based on derivatives (backpropagation).

2.3.1 Configuration ANFIS-A

The neuro-fuzzy system designed consists of 7 inputs, 1 output and 128 rules, 2 membership functions in each input. Figure-14 shows the structure of the neuro-fuzzy system. Figure-15 shows the membership functions used in the inputs. Other features are:

- Number of nodes: 294
- Number of linear parameters: 1024
- Number of nonlinear parameters: 42
- Total number of parameters: 1066
- Number of fuzzy rules: 128

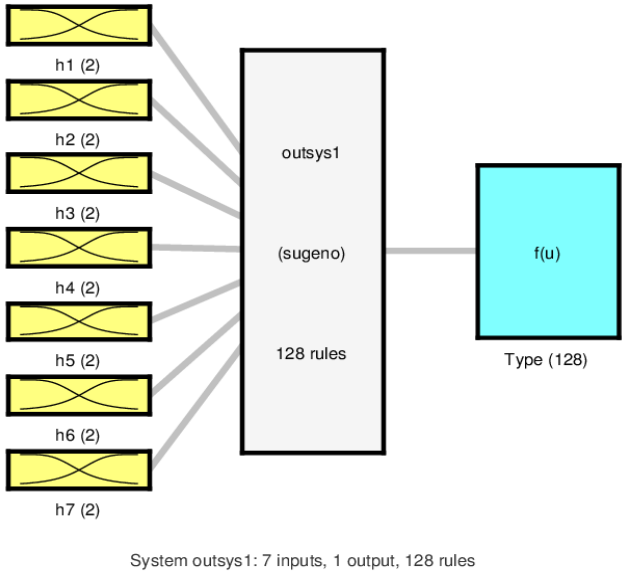

Figure-14. Neuro-fuzzy system designed: ANFIS-A, with 7 inputs (Hu's moments), 1 output (Result of classification) and 128 rules of classification.

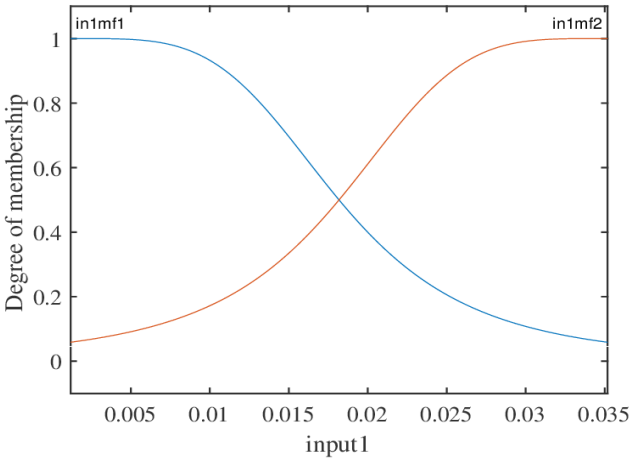

Figure-15. Example of fuzzy sets used for each input for configuration ANFIS-A.

The labels in1mf1 and in1mf2 represent the segmentation that is made of the universe of input where they can be associated with values: Low, Medium and High. They allow the generation of rules considering the possible values, for example: If a value of the moment of Huh_1 is low (in1mf1) then the possibility that the patient presents cancer is (high or low) depending on the case and the dataset.

2.3.2 Configuration ANFIS-B

In this case, the neuro-fuzzy system consists of 7 inputs, 1 output 3 membership functions in each input; the respective structure is shown in Figure-16 and the membership functions used in Figure-17.

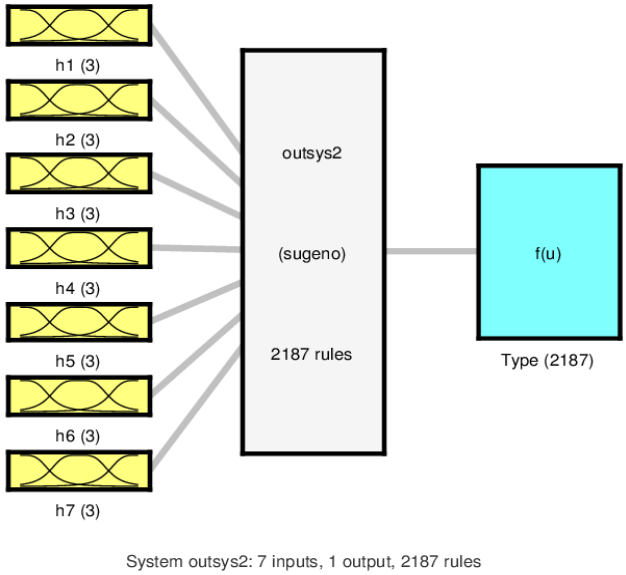

Figure-16. Neuro-fuzzy system designed: ANFIS-B, with 7 inputs (Hu's moments), 1 output (Result of classification) and 2187 rules of classification.

Considering the structure of the neuro-fuzzy system shown in figure 16, the other parameters are:

- Number of nodes: 4426
- Number of linear parameters: 17496
- Number of nonlinear parameters: 42
- Total number of parameters: 17538
- Number of fuzzy rules: 2187

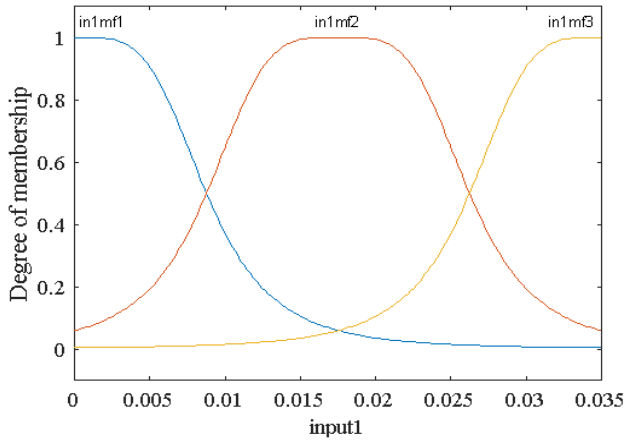

Figure-17. Example membership functions used in the inputs for configuration ANFIS-B.

3. RESULTS

The algorithms were implemented using MATLAB 2018b since they provide a set of ready-to-use and easy-to-use tools for generating a first prototype. The computer used had 12 GB of RAM, Intel Core I7-4700MQ CPU 2.4GHz x 8 GEFORCE GT 740M / PCIe / SSE2 Graphic Card.

The implementation of experimental cases considering the configurations ANFIS-A and ANFIS-B, also is used the total dada and a case were the data was balanced for training process. The experimental cases are:

- Experimental case 1: Using ANFIS-A model and total data.
- Experimental case 2: Using ANFIS-A model and reduced balanced data.
- Experimental case 3: Using ANFIS-B model and reduced balanced data.

It is noticeable that for experimental case 2 and 3, the total image of healthy and unhealthy was taken in a similar proportion (reduced balanced data); however, for testing was used the total data. The respective sets of data are:

- Configuration using total data: healthy = 1424, unhealthy = 198, total = 1622.
- Configuration reduced balanced data: healthy = 198, unhealthy = 198, total = 396.

A confusion matrix is considered to establish the performance obtained in each case as presented in Table-1, which contains the correct and incorrect identification number for healthy and unhealthy images.

Table-1. Description of the generic confusion matrix.

-	**Healthy**	**Unhealthy**	**Total images**
Healthy	Correct healthy	Incorrect unhealthy	1424
Unhealthy	Incorrect healthy	Correct unhealthy	198

3.1 Experimental Case 1

The performance function used for training process is the Root Mean Square Error (RMSE), after the training process the minimal training RMSE is 0.565194. The other characteristics of training process are:

- Total unhealthy images 198
- Correct unhealthy classified = 56
- Incorrect unhealthy classified = 142
- Total healthy images = 1424
- Correct healthy classified = 1407
- Incorrect healthy classified = 17

The respective confusion matrix obtained in this case is presented in Table-2. Given the results of ANFIS it can be seen that the correct classifications obtaining a success rate of the neuro-fuzzy system of 90.2%, achieves a correct classification of 1407 healthy images and 56 for unhealthy.

Table-2. Confusion matrix obtained for case 1.

-	Healthy	Unhealthy	Total images
Healthy	1407	17	1424
Unhealthy	142	56	198

3.2 Experimental Case 2

Checking the results case 1 it is observable that there is an over fitting in positive classifications in healthy images, this is due the amount of images used to train the classifier, for that reason in the second experiment the classifier is trained with the same proportion of healthy and unhealthy images obtaining the confusion matrix of Table-3, achieving a correct classification of 1357 healthy images and 198 for unhealthy. Additionally, after the training process the minimal training RMSE is 0.881088.

Table-3. Confusion matrix obtained for case 2.

-	Healthy	Unhealthy	Total images
Healthy	1357	67	1424
Unhealthy	102	96	198

3.3 Experimental Case 3

As third configuration, ANFIS was implemented with three membership functions of each input. After the training process the minimal training RMSE is 0.868317. The results of this configuration are shown in Table 4. In this case is obtained a correct classification of 1389 healthy images and 198 for unhealthy.

Table-4. Confusion matrix for case 3.

-	Healthy	Unhealthy	Total images
Healthy	1389	35	1424
Unhealthy	100	98	198

3.4 Comparison

This part presents the comparison of the results obtained in the experimental cases. Given the last results, the following indicators are computed to give comparative results in Table-5. The best accuracy, error rate and sensitivity are obtained for case 3, and the best specificity and precision for case 1. The indicators presented in table 5 are calculated as:

$$\text{Accuracy} = \frac{\text{Correct healthy + Correct unhealthy}}{\text{Total figures}} \quad (2)$$

$$\text{Error rate} = \frac{\text{Incorrect healthy +Incorrect unhealthy}}{\text{Total figures}} \quad (3)$$

$$\text{Sensitivity} = \frac{\text{Correct unhealthy}}{\text{Total unhealthy}} \quad (4)$$

$$\text{Sensitivity} = \frac{\text{Correct healthy}}{\text{Correct healthy + Incorrect unhealthy}} \quad (5)$$

$$\text{Precision} = \frac{\text{Correct unhealthy}}{\text{Correct unhealthy + Incorrect unhealthy}} \quad (6)$$

Table-5. Performance indicators computed from matrices of confusion shown in Tables 2, 3 and 4.

-	Accuracy	Error rate	Sensitivity	Specificity	Precision
Case 1	0.90196	0.09802	0.28282	0.98805	0.76712
Case 2	0.8958	0.10419	0.48485	0.95294	0.76712
Case 3	0.91676	0.08322	0.49495	0.97542	0.73683

Considering this results, it is noticeable the importance of a suitable method for detecting a cancer case. Where a mistake in a healthy identification can be handled via other diagnostic exams, however a mistake in an unhealthy case is dangerous because it does not provide the alternative to perform others diagnostic exams.

According to Table-5, it is created the ROC Receiver Operating Characteristic curve shown in Figure-18. The ROC is plotted using true positive rate (y-axes) in function of the false positive rate (x-axes) for different points [20], in which the area under the curve is 84% which represents the Confidence Interval for sensitivity/specificity, likelihood ratio and predictive values.

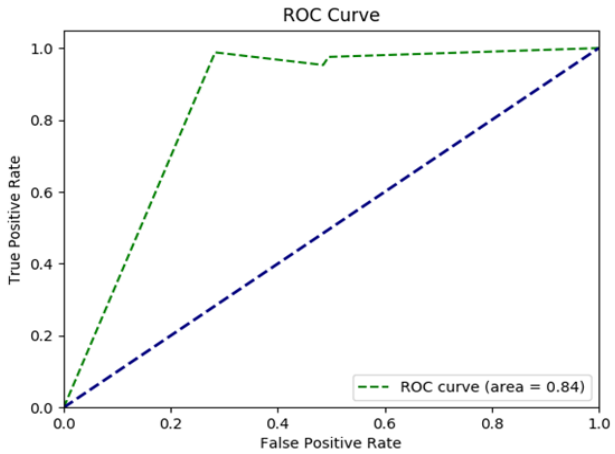

Figure-18. ROC Curve for the three configurations of the implemented fuzzy system.

4. CONCLUSIONS

The model created using ANFIS provides a suitable system for the detection of Uveal Melanoma obtaining results with the first configuration of 90.2% accuracy, although this configuration produces high accuracy, it also produces a low sensitivity 28.3%. This problem was solved with configuration two, reducing the healthy training images to avoid an over-fitting although the accuracy was reduced. Finally, with configuration 3 it is achieved an accuracy of 91.68%, a high specificity and the best sensitivity in the three configurations proposed; all of the measures mentioned above are with an optimal of 84% confidence interval.

Considering the results is more important the identification of an unhealthy case than the healthy cases. Then, the design of the fuzzy identification system can incorporate this feature. Reducing the size of healthy images for training reduce the over fitting to classify healthy images, increasing the success rate to detect unhealthy images but reducing the success rate for unhealthy images.

In a future work the model using a computer with high features will be tested expecting to have more precise results using multiple membership functions in ANFIS. For allowing mayor interpretability it is possible to consider extending the TSK fuzzy system to a Mamdani fuzzy system.

It is expected to test the proposed system as an assistance system for diagnosis of Uveal Melanoma, for that reason, the prototype implemented in MATLAB will be migrated to another programming language such as Python or Java, so that this system can be implemented on Smart-phones, Raspberry Pi or any other digital processing device.

ACKNOWLEDGMENTS

Institute of Automation Chinese Academy of Science for providing the CASIA Dataset, Universidad Distrital Francisco José de Caldas and Dr. Paul T. Finger, MD.

REFERENCES

[1] National Cancer Institute, Cancer Statistics. 2018. [Online], Available: https://www.cancer.gov/espanol/cancer/naturaleza/estadisticas.

[2] M. Zaharia. 2013. Cancer as a public health problem in Peru, Revista Peruana de Medicina Experimental y Salud Pública. 30(1): 7-8.

[3] A.B. Miller. 1995. An epidemiological perspective on cancer screening, Clin Biochem. 28(1).

[4] B.A. Krantz, N. Dave, K.M. Komatsubara, B.P. Marr, R.D. Carvajal. 2017. Uveal melanoma: epidemiology, etiology, and treatment of primarydisease, Clin Ophthalmol. 11: 279-289.

[5] American Cancer Society. 2018. Eye Cancer Survival Rates, [Online], Accessed on 20 Sep, Available: https://www.cancer.org/cancer/eyecancer/detection-diagnosis-staging/survival-rates.htmlreferences.

[6] P. Perner. 2014. Iris Acquisition and Detection for Computer-assisted Iridiology, IEEE 22nd Signal Processing and Communications Applications Conference (SIU).

[7] S. Amerifar, A.T. Targhi, M.M. Dehshibi. 2015. Iris the picture of health: Towards medical diagnosis of diseasesbasedon iris pattern, The Tenth International Conference on Digital Information Management (ICDIM).

[8] G. Durga-Devi, D.M.D Preethi. 2014. Diseaseidentification in iris usinggaborfilter, International Journal of Engineering and Computer Science. 3: 5369-5399.

[9] A.D. Wibawa, M.A.R. Sitorus, M.H. Purnomo. 2016. Classification of iris image of patientchronic renal failure (crf) using watershed algorithm and support vector machine (svm), Journal of Theoretical and AppliedInformationTechnology. 19(2).

[10] S. Kaliki, C.L. Shields. 2017. Uveal melanoma: relative lyrarebutdeadlycancer, Eye (Lond). 31(2): 241-257.

[11] L.X. Wang. 1997. A courseon Fuzzy Systems and Control, Prentice Hall, Upper Saddle River, NJ.

[12] B.M. del Brío, A.S. Molina. 2006. Redes Neuronales y Sistemas Difuso, Alfaomega, Segunda Edición.

[13] R. Babuska. 1998. Fuzzy Modeling for Control, Wiley, London, England.

[14] J.S.R Jang, C.T. Sun, E. Mizutani. 1997. Neuro-Fuzzy and Soft Computing: A Computational Approach to Learning and Machine Intelligence, Prentice Hall.

[15] M. Yousefia, D. Hooshyarb, A. Ramezanib, K. Salleh, W. Khaksara, Firas B. Ismail Alnaimi. 2015. Short-termwindspeedforecastingbyan adaptive network-based fuzzy inferencesystem (ANFIS): an attempt to wardsanensemble forecasting method, International Journal of Advances In Intelligent Informatics. 1(3): 140-149.

[16] M. A.Boyacioglu, D. Avci. 2010. AnAdaptive Network-Based FuzzyInference System (ANFIS) fortheprediction of stock marketreturn: The case of theIstanbul Stock Exchange, Expert Systems with Applications. 37(12): 7908-7912.

[17] A. Bermudez, J.A. Lugo, P.Y. Piñero. 2015. An Adaptive-Network-Based Fuzzy Inference System for Project Evaluation. 19(2): 53-67.

[18] L.-C. Ying, M.-C. Pan. 2008. Using adaptive network based fuzzy inferencesystemtoforecast regional electricityloads, Energy Conversion and Management. 49(2): 205-211.

[19] Z. Yang, Y. Wang, G. Ouyang. Adaptive Neuro-Fuzzy Inference System for Classification of Background EEG Signals from ESES Patients and Controls, The Scientific World Journal. Vol. 2014.

[20] Center for Biometrics and Security Research, Institute of Automation, Chinese Academy of Sciences, [Online], Accessedon 20 Sep, 2018, Available: http://www.cbsr.ia.ac.cn/english/IrisDatabase.asp

[21] New York eyecancer center, [Online], Accessedon: Sep, 2018, Available: https://eyecancer.com/eyecancer/conditions/iris-tumors/iris-melanoma.

[22] P. Roy, S. Dutta, N. Dey, G. Dey, S. Chakraborty, R. Ray. 2014. Adaptivethresholding: A comparative study, International Conference on Control, Instrumentation, Communication and Computational Technologies (ICCICCT).

[23] S. Just. 2017. Circular Hough transform, [Online], Accessedon: Sep, 2017, Available: https://cdn.manesht.ir/9961_Simon_Pedersen_CircularHoughTransform.pdf

[24] Z. Huang, J. Leng. 2010. Analysis of Hu'smomentinvariantsonimagescaling and rotation, 2nd International Conference on Computer Engineering and Technology (ICCET).

[25] J. Cerda, L. Cifuentes. 2012. Uso de curvas ROC en investigación clínica. Aspectos teórico-prácticos, Revista chilena de infectología. 29(2): 138-141.